MEDICAL SCIENCE MONITOR

CLINICAL RESEARCH

e-ISSN 1643-3750
© Med Sci Monit, 2019; 25: 8379-8388
DOI: 10.12659/MSM.918489

Received: 2019.07.03
Accepted: 2019.09.25
Published: 2019.11.07

# Biomechanical Comparison of Optimal Shapes for the Cervical Intervertebral Fusion Cage for C5–C6 Cervical Fusion Using the Anterior Cervical Plate and Cage (ACPC) Fixation System: A Finite Element Analysis

Authors' Contribution:
Study Design A
Data Collection B
Statistical Analysis C
Data Interpretation D
Manuscript Preparation E
Literature Search F
Funds Collection G

A 1,2 Jiajia Wang
B 2 Zhihui Qian
B 2 Luquan Ren

1 College of Agricultural Equipment Engineering, Henan University of Science and Technology, Luoyang, Henan, P.R. China
2 Key Laboratory of Bionic Engineering (Ministry of Education, China), Jilin University, Changchun, Jilin, P.R. China

**Corresponding Author:** Zhihui Qian, e-mail: zhq@jlu.edu.cn
**Source of support:** This study was supported by the Project of Scientific and Technological Cooperation between China and Italy (No. 2016YFE0103700) and the Fundamental Research Funds of China (No. Z201105)

**Background:** The fifth and sixth cervical vertebrae (C5–C6) represent the high-risk segment requiring surgical correction in cervical spondylosis. Anterior cervical discectomy and fusion (ACDF) of C5–C6 includes an intervertebral fusion cage to maintain foraminal height and is combined with anterior plate fixation. The shape of the intervertebral cage can affect the postoperative outcome, including the rates of fusion, subsidence, and neck pain. This study aimed to use finite element (FE) parametric analysis to compare biomechanical properties of changes in intervertebral cage shape for C5–C6 cervical fusion using the anterior cervical plate and cage (ACPC) fixation system.

**Material/Methods:** Five shapes were designed for cervical intervertebral cages, square, oval, kidney-shaped, clover-shaped, and 12-leaf-shaped. The performance was evaluated following implantation into the validated normal C5–C6 FE model using simulation with five physiological conditions. The indicators included the maximum von Mises stress of the endplates, the fusion cages, and the cervical vertebrae. The postoperative subsidence-resistance properties were determined, including the interior stress responses of the intervertebral cages and the surrounding tissues. The fusion-promoting properties were evaluated by the interior stress responses of the bone grafts.

**Results:** The optimal shape of the cervical intervertebral cage was the 12-leaf-shape for postoperative subsidence resistance. The kidney shape for the cervical intervertebral cage was optimal for postoperative fusion.

**Conclusions:** FE analysis identified the optimal cervical intervertebral cage design for ACPC fixation of C5–C6. This method may be useful for future developments in the design of spinal implants.

**MeSH Keywords:** Finite Element Analysis • Infusions, Spinal • Postoperative Complications • Prostheses and Implants

**Full-text PDF:** https://www.medscimonit.com/abstract/index/idArt/918489







Indexed in: [Current Contents/Clinical Medicine] [SCI Expanded] [ISI Alerting System] [ISI Journals Master List] [Index Medicus/MEDLINE] [EMBASE/Excerpta Medica] [Chemical Abstracts/CAS]

## Background

Anterior fusion surgery is widely used for patients with cervical intervertebral disc herniation and severe cervical spondylosis myelopathy requiring cervical vertebral decompression and fusion [1,2]. The prevention of postoperative complications of surgical correction in cervical spondylosis has attracted increasing research attention [3–5]. Anterior cervical discectomy and fusion (ACDF) procedures with anterior plate fixation have resulted in superior surgical outcomes, including increased rates of fusion and reduced rates of subsidence [6]. Midterm follow-up of the clinical and radiological results achieved by tantalum intervertebral fusion cages for single-level ACDF have shown that the cages remain in good condition for up to 11 years postoperatively, and similar results with the use of autologous bone grafts and plating were also reported [7]. The use of plates and fusion cages with screws can promote fusion, but no clinically significant differences have been shown [8]. Kettler et al. [9] reported that the design of the implants used determines the relationship between the activity and the subsidence rate. The vertical ring-shaped intervertebral cage is one of the most effective designs [10]. However, further studies are needed to determine how the design and shape of the fusion cage can influence the postoperative outcome.

Tan et al. [11] showed that the cloverleaf, or 4-leaf-shape, interbody cage provided higher interface bonding strength when compared with kidney-shaped and elliptical interbody cages. Among all these cage designs, the ring-shaped cervical intervertebral fusion cage has biomechanical advantages over other designs, and studies have shown that the shape of the cage influences the mechanical properties and postoperative outcome [10,12,13]. In 2013, Hsu [14] optimized the shape of the interbody cervical cage using simulation-based methods followed by experimental verification and obtained an optimal flower-shaped design, which reduced the rate of postoperative subsidence. However, the postoperative effects of the shapes of cervical intervertebral fusion cages under physiological conditions have not been investigated.

Due to the difficulty in obtaining internal stress information from traditional biomechanical cadaveric studies or *in vivo* animal experiments, this study aimed use parametric finite element (FE) analysis and modeling to compare the biomechanical properties of changes in intervertebral fusion cage shape for C5–C6 cervical fusion using the anterior cervical plate and cage (ACPC) fixation system.

## Material and Methods

### Establishment and validation of the finite element (FE) model

The fifth and sixth cervical vertebral levels (C5–C6) were extracted from the previously reported cervical finite element (FE) model [15]. The fixed element (FE) model of the vertebra consists of an inferior endplate, a superior endplate, a cancellous core, a cortical wall, and a posterior structure. Seven intervertebral ligaments, including the ligamentum flavum, the supraspinous ligament, the interspinous ligament, the anterior longitudinal ligament, the transverse ligament, the posterior longitudinal ligament, and the capsular ligament were modeled anatomically. The intervertebral discs consist of both the nucleus pulposus and the annulus fibrosus. The material properties of the vertebra, ligaments, and annulus fibrosus were acquired from previously published studies (Table 1) [16–18]. The nucleus pulposus was treated as an incompressible solid element, and its volume was one-third of the disc volume [19]. We treated the facet joints as frictionless surface-to-surface contact elements in the simulation [16,20].

The C5–C6 model was validated through comparison with published experimental data under physiological motion patterns. The boundary conditions and loading conditions of the validation model were obtained from previously published studies [21–26]. All nodes on the base of the sixth cervical level were fixed in six degrees of freedom. Firstly, the 1 mm axial displacement load was exerted on the upper surface of the vertebral body of C5. The force-displacement curve of the C5 vertebral body (base) was obtained and compared with the results from human cadaveric data obtained by Shea et al. [21], Yoganandan et al. [22], and Heitplatz et al. [23] and the simulation data provided by Teo et al. [24] (Figure 1). Secondly, the moment of 1.8 Newton meter (N·m) was exerted on the upper surface of the C5 vertebral body under four types of motion patterns, including flexion, extension, lateral bending, and axial rotation. The intervertebral rotation data were compared with previously reported *in vitro* experimental data (Table 2) [25,26]. The predicted range of motion of the C5–C6 segmental model was consistent with *in vitro* experimental data and the predicted results using published models.

According to the requirements of anterior cervical surgery, the anterior longitudinal ligament and pathological intervertebral disc were removed and prepared for cervical intervertebral cage implantation. The Orion static locking plate (Medtronic Sofamor Danek, Minneapolis, MN, USA) was used in this study as it was easy to operate and resulted in firm fixation. The dimensional parameters of the Orion plate and screw were determined according to the detailed dimensional parameters of the cervical intervertebral space identified in this study.





Indexed in: [Current Contents/Clinical Medicine] [SCI Expanded] [ISI Alerting System] [ISI Journals Master List] [Index Medicus/MEDLINE] [EMBASE/Excerpta Medica] [Chemical Abstracts/CAS]

**Table 1.** The material properties and element type defined in the C5–C6 finite element (FE) model.

| Component | Element type | Density (Ton/mm³) | Young's modulus (MPa) | Poissson's ratio | Cross-section area (mm²) |
|---|---|---|---|---|---|
| Cortical bone | Trilateral | 1.83E-09 | 12000.0 | 0.29 | – |
| Cancellous bone | Tetrahedral | 1.00E-09 | 450.0 | 0.29 | – |
| posterior structure | Tetrahedral | 1.83E-09 | 3500.0 | 0.29 | – |
| Annulus | Tetrahedral | 1.20E-09 | 3.4 | 0.40 | – |
| Nucleus | Tetrahedral | 1.36E-09 | 1.0 | 0.49 | – |
| Endplate | Trilateral | 1.83E-09 | 12000.0 | 0.29 | – |
| Anterior Longitudinal ligament | Truss | 1.10E-09 | 30.0 | 0.40 | 6.1 |
| Posterior longitudinal ligament | Truss | 1.10E-09 | 20.0 | 0.40 | 5.4 |
| Ligamentum flavum | Truss | 1.10E-09 | 10.0 | 0.40 | 50.1 |
| Supraspinous ligament | Truss | 1.10E-09 | 1.5 | 0.40 | 13.1 |
| Interspinous ligament | Truss | 1.10E-09 | 10.0 | 0.40 | 13.1 |
| Capsular ligament | Truss | 1.10E-09 | 10.0 | 0.40 | 46.6 |
| Transverse ligament | Truss | 1.10E-09 | 20.0 | 0.40 | 15.0 |

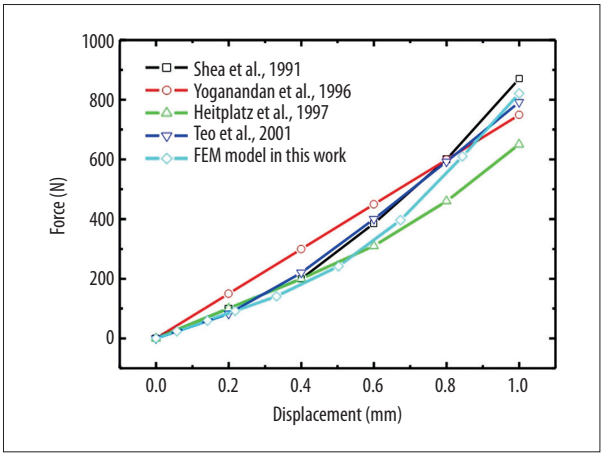


**Figure 1.** Force-displacement curves of the finite element (FE) model established in the present study compared with previously published results.

CATIA V5R13 software (Dassault Systèmes, Paris, France) was used for geometric modeling, and HyperMesh software for FE modeling (Altair, Troy, MI, USA) was used for mesh generation (Figure 2). Figure 3 shows the C5–C6 FE model with the implantation of the steel plate and screw. The screw-vertebra interface was defined as the tie constraint. The interfaces between the endplate and fusion cage and the endplate and bone graft were defined as the nonlinear node-surface contact, with a friction coefficient of 0.07 [27]. The boundary condition was fixed at the six degrees of freedom of the nodes at the base of the C6 vertebra. Gravity was added by exerting 52.5 N force and a moment of 1.8 N·m with gravity on the superior surface of the C5 vertebral body to investigate the performance of the vertebra during flexion, extension, lateral bending, and axial rotation. The simulation was performed using the ABAQUS/Standard module of ABAQUS version 6.91 software (Simulia, Dassault Systèmes, Paris, France).

**Table 2.** Simulated rotational data of the finite element (FE) model in the present study compared with previously published results.

| Moment/1.8N·m | Intervertebral rotation of the C5–C6 segment (°) | | |
|---|---|---|---|
| | *In vitro* experimental results of Moroney et al. | FE simulation results of Teo et al. | FE simulation results of this work |
| Flexion | 5.55±1.84 | 4.02 | 3.45 |
| Extension | 3.52±1.94 | 3.82 | 4.39 |
| Lateral bending | 4.71±2.99 | 3.16 | 1.81 |
| Axial rotation | 1.85±0.67 | 1.48 | 2.15 |





Indexed in: [Current Contents/Clinical Medicine] [SCI Expanded] [ISI Alerting System] [ISI Journals Master List] [Index Medicus/MEDLINE] [EMBASE/Excerpta Medica] [Chemical Abstracts/CAS]

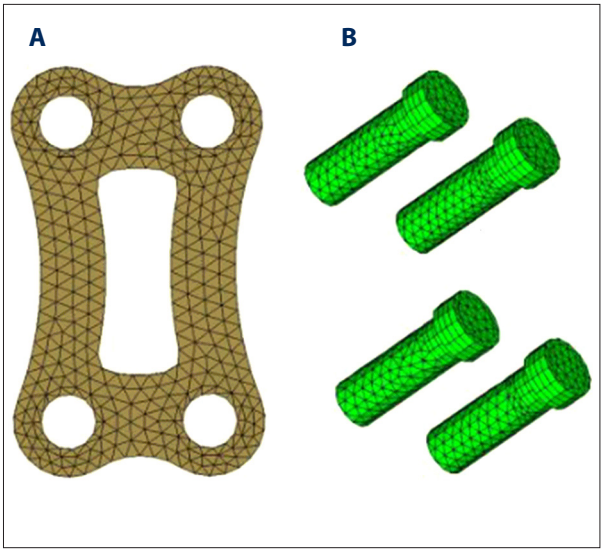


**Figure 2.** Models of the fixed plate (**A**) and screw (**B**).

### Design of the fusion cages with five different surface shapes

In this study, five vertical ring cervical intervertebral fusion cages were designed with different shapes that were designed based on designs previously reported by Tan et al. [11] and Hsu et al. [14]. The cage shapes were square, oval, kidney-shaped, clover-shaped (4-leaf-shaped), and 12-leaf-shaped. The following geometric sizes of the fusion cages were set according to the real-world measurement data based on the model. Firstly, the distance between the vertebral uncinate processes was 15.8 mm for C5 and 15.0 mm for C6. The accommodated width of the fusion cage was <14.0 mm. The coronal distance was set as 13.0 mm. Second, the sagittal vertebral diameter was 17.5 mm. The anterior and posterior safe distances were set at 1.5 and 3.0 mm, respectively, to prevent the backward protrusion of the fusion cage and damage to the spinal canal. Therefore, the sagittal diameter of the fusion cage was set as 13.0 mm. Thirdly, the vertebral spaces between the superior and inferior vertebral bodies were 3.8 mm anteriorly, 5.0 mm in the middle, and 4.0 mm posteriorly. The height of the fusion cage was set as 5.0 mm for effective decompression.

In conclusion, the length, width, and height of the fusion cage were 13 mm, 13 mm, and 5 mm, respectively. The surface areas of the fusion cages were set as the same to eliminate the influence of surface area changes. Also, the contact areas between the fusion cage and adjacent endplates were required to be 30–40% of the endplate area to ensure adequate supporting strength of the cage [28,29]. Measurement with the FE model showed that the endplate areas of the C5 and C6 vertebral inferior surface were 220.8 $mm^2$ and 260.7 $mm^2$, respectively. Also, a 5 mm-diameter hole was drilled in the center of the fusion cage to accommodate the bone graft and to ensure better fusion effects between the cage and adjacent vertebral bodies.

The surface areas of the fusion cage met the criteria of the following equation:

$$S = S_{\text{fusion cage}} + S_{\text{bone graft}} \quad (1)$$

The contact area between the fusion cage and adjacent superior or inferior endplates met the criteria of the following equation:

$$S_{\text{fusion cage}} \geq 260.686 \times 30\% = 78.206\ mm^2 \quad (2)$$

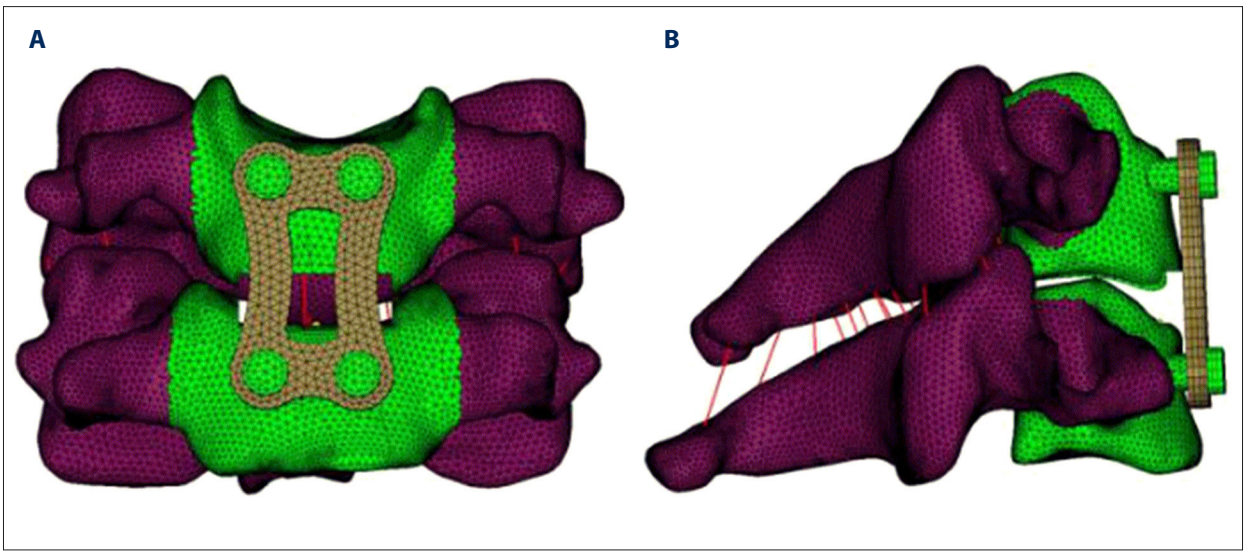


**Figure 3.** Front view (**A**) and left view (**B**) of the finite element (FE) model with fixed plate and screw.





Indexed in: [Current Contents/Clinical Medicine] [SCI Expanded] [ISI Alerting System] [ISI Journals Master List] [Index Medicus/MEDLINE] [EMBASE/Excerpta Medica] [Chemical Abstracts/CAS]

**Table 3.** The cage area and the percentage of the area occupied of the total cage area.

| Shape design | Cage area ($mm^2$) | Area (%) |
|---|---|---|
| Square | 90.615 | 34.8% |
| Oval | 92.623 | 35.5% |
| Kidney | 89.805 | 34.4% |
| Clover (4-leaf-shape) | 93.251 | 35.8% |
| 12-leaf-shape | 91.926 | 35.3% |

**Table 4.** Material properties of the model.

| Cage/bone graft material | Elastic modulus (MPa) | Poisson ratio |
|---|---|---|
| Ti/Ti alloy [26] | 100,000.00 | 0.30 |
| Bone graft [30] | 3,500.00 | 0.30 |

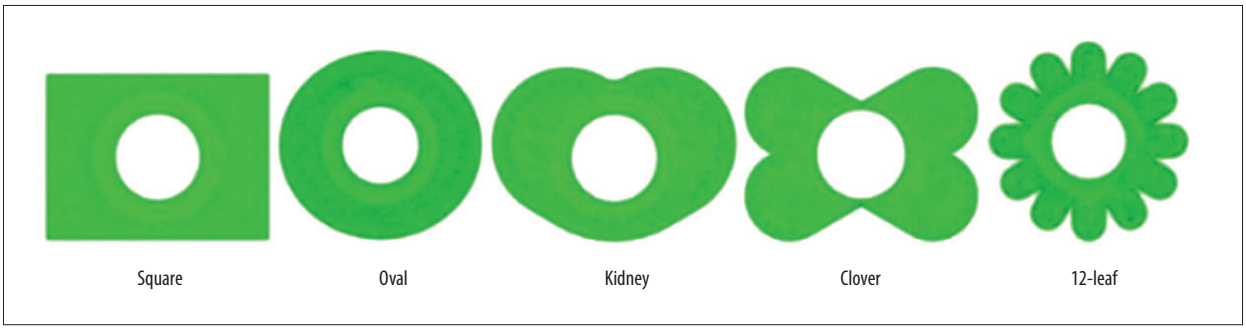


**Figure 4.** Five shapes were designed for cervical intervertebral cages, square, oval, kidney-shaped, clover-shaped, and 12-leaf-shaped.

Table 3 shows the surface area and the percentage of the total endplate area. Figure 4 shows the five cervical intervertebral fusion cage models. The materials of the fusion cage and anterior equipment were set using titanium alloy, and the material of the bone graft was set using cancellous bone, as shown in Table 4.

### Evaluation of the effects of the implant on adjacent tissues

This study aimed to investigate the postoperative effects of implantation of the cervical intervertebral fusion cage under normal physiological motion patterns, including natural gravity and front flexion, extension, lateral bending, and axial rotation. The stresses distributed on the endplate, fusion cage, and vertebrae were used to evaluate the possibility of subsidence. As described by Wolff's Law, that remodeling and growth of bone are in response to the applied forces, appropriate stress stimulation on bone grafts is beneficial for bone growth. The immediate biomechanical stability of the anterior fusion cages would be maintained through a plate system. Therefore, because increased stress on the inner bone graft might improve the postoperative fusion effect, bone graft stress was used to evaluate the possibility that it promoted bone fusion.

## Results

### The finite element (FE) simulation results

Figure 5 shows that the simulation results included the changes in the indicators of subsidence in the five shapes of the fusion cages under five physiological conditions. The indicators included the maximum von Mises stress of the endplates, the fusion cages, and the vertebrae. The vertebrae included the C5 vertebral cancellous bone (C5-cancellous bone), C6 vertebral cancellous bone (C6-cancellous bone), C5 vertebral cortical bone (C5-cortical bone), and C6 vertebral cortical bone (C6-cortical bone).

### Evaluation of anti-subsidence properties

Overall, stresses were less in axial compression and the forward bending movement mode but were greater in the motion patterns of extension, rotation, and lateral bending. The results showed that the possibility of subsidence under extension, lateral bending, and rotation motion were less than for forward bending and the static state.

Figure 5A shows that when the maximum stress of endplate was considered as the optimum index, two fusion cages with the 12-leaf and the oval shapes resulted in greater performance in resistance to subsidence.





Indexed in: [Current Contents/Clinical Medicine] [SCI Expanded] [ISI Alerting System] [ISI Journals Master List] [Index Medicus/MEDLINE] [EMBASE/Excerpta Medica] [Chemical Abstracts/CAS]

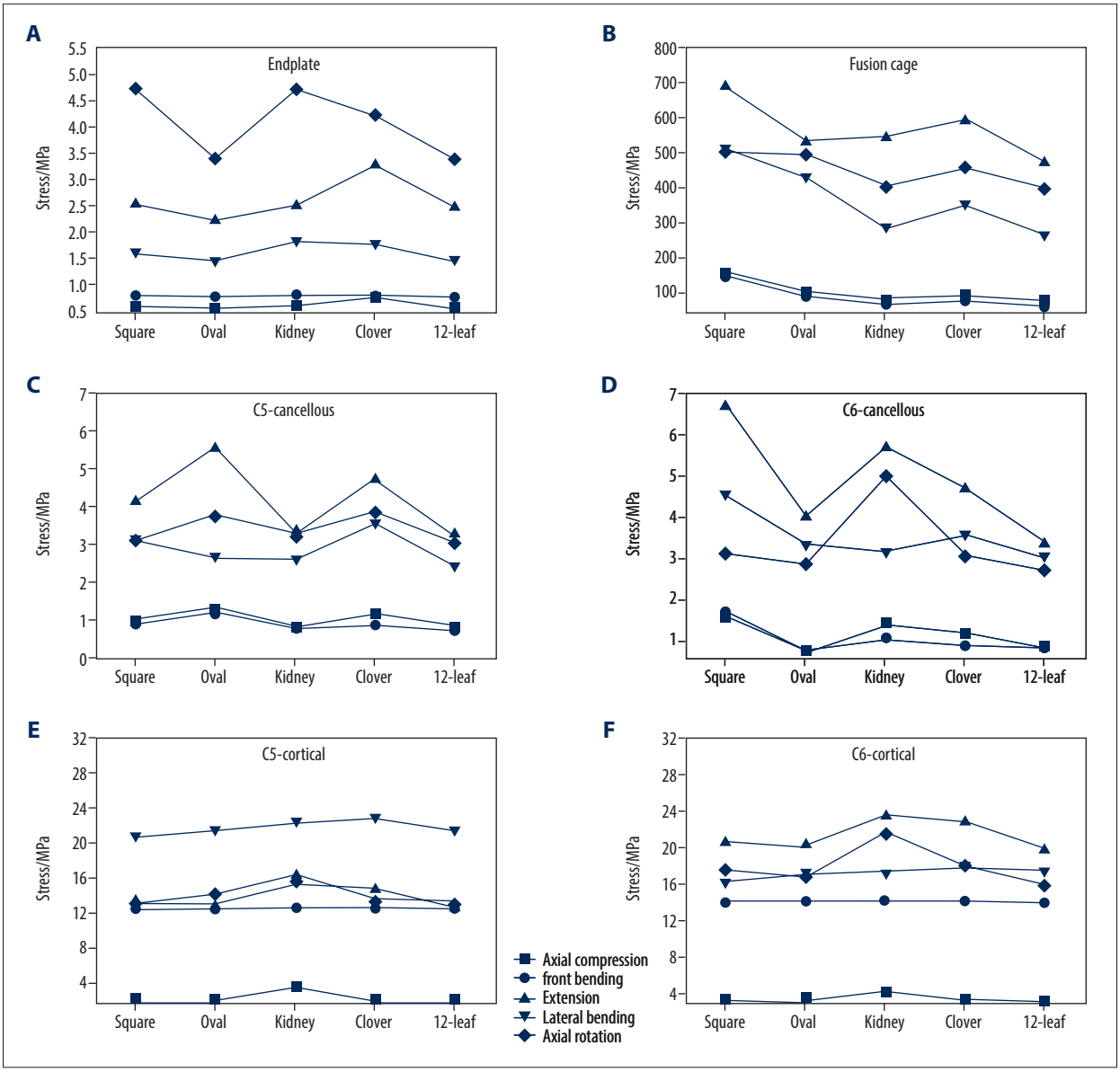


**Figure 5.** (**A–F**) Simulated results of subsidence-resistant properties.

Figure 5B shows that when the maximum stress of the cage was considered at the optimum index, the two fusion cages with the 12-leaf and kidney shapes resulted in greater performance in resistance to subsidence. Figure 5C and 5D show that when the maximum stress value of the cancellous bone was taken into account in the optimizing index, three shapes of cage resulted in a greater performance in the resistance to subsidence, including the 12-leaf, the kidney, and the oval shapes. Figure 5E and 5F show that when the maximum stress value in cortical bone was used as the optimization index, three shapes of cage showed increased performance in the prevention of subsidence, which were the 12-leaf, the square, and the oval shapes. Overall, the fusion cage with 12-leaf and oval shapes resulted in improved resistance to subsidence.

### Performance evaluation of bone graft fusion

Figure 6 shows the maximum bone graft von Mises stress values calculated from the five shapes of fusion cages in five modes. The stress on the bone graft in the extension movement was maximal, followed by the rotation movement, lateral bending, and the axial movement. The extension motion pattern was suitable for bone graft fusion. Two types of fusion that included the clover shape and the kidney shape resulted in greater bone graft stress.





Indexed in: [Current Contents/Clinical Medicine] [SCI Expanded] [ISI Alerting System] [ISI Journals Master List] [Index Medicus/MEDLINE] [EMBASE/Excerpta Medica] [Chemical Abstracts/CAS]

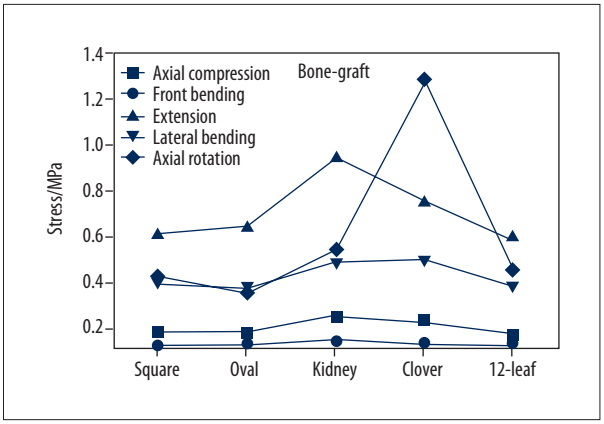


**Figure 6.** Maximum von Mises stress on the bone grafts.

### Stress distribution

A previously published study reported that following anterior discectomy with a loose graft, there was increased motion postoperatively, and although a tight-fitting graft reduced motion, stress could increase beyond the strength of the graft [30]. In the present study, the results showed that the motion pattern could be associated with subsidence in the extension motion mode. The stress distribution of different shapes of fusion cages in the extension motion mode is shown in Figures 7–10. Figure 7 shows the maximal stress distribution in the endplate. The endplate stress distribution of the square, clover, and 12-leaf shapes of the cage was more uniform compared with the oval, and kidney shape with no significant concentration phenomenon.

Figure 8 shows the surface stress distribution in the extension movement condition for the different shapes of the fusion cages. In accordance with the corresponding endplate stress distribution location, larger stress was mainly distributed on the edge of the cage. Figure 9 shows the stress distribution of cancellous bone and cortical bone between different shapes of fusion cages in the extension motion mode. For the C5 cancellous bone, the stress of 12-leaf and oval shapes of fusion cages were well distributed. For the C6 cancellous bone, the stress distribution of 12-leaf and kidney shapes of fusion cages were homogeneous.

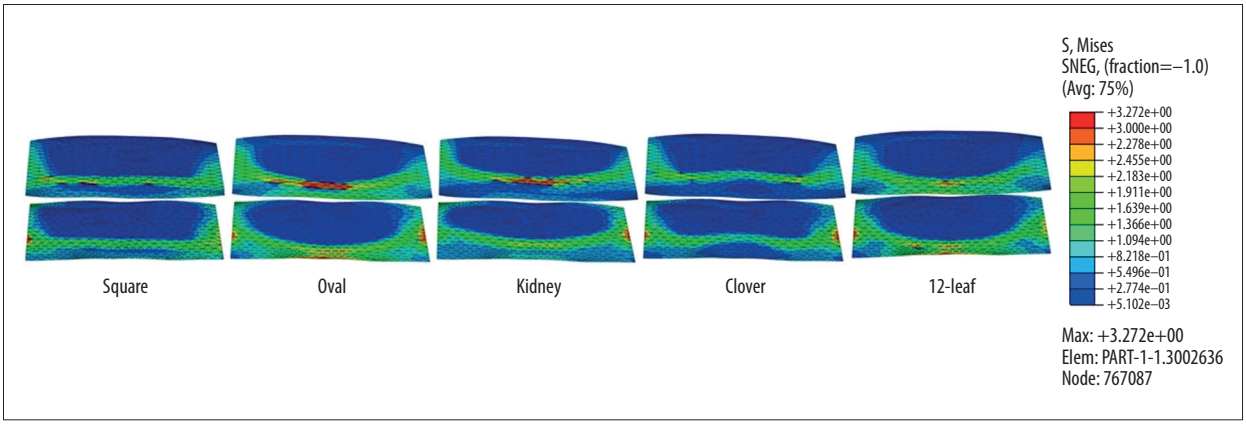


**Figure 7.** Stress distribution on endplates of the five shapes of the cervical intervertebral cages in the extension motion condition.

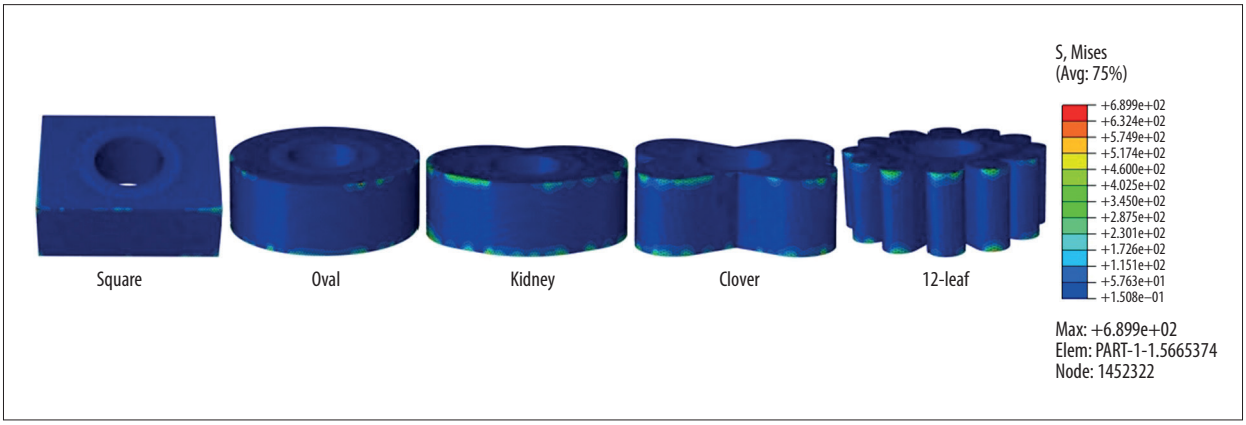


**Figure 8.** Stress distribution on the five shapes of the cervical intervertebral cages in the extension motion condition.





Indexed in: [Current Contents/Clinical Medicine] [SCI Expanded] [ISI Alerting System] [ISI Journals Master List] [Index Medicus/MEDLINE] [EMBASE/Excerpta Medica] [Chemical Abstracts/CAS]

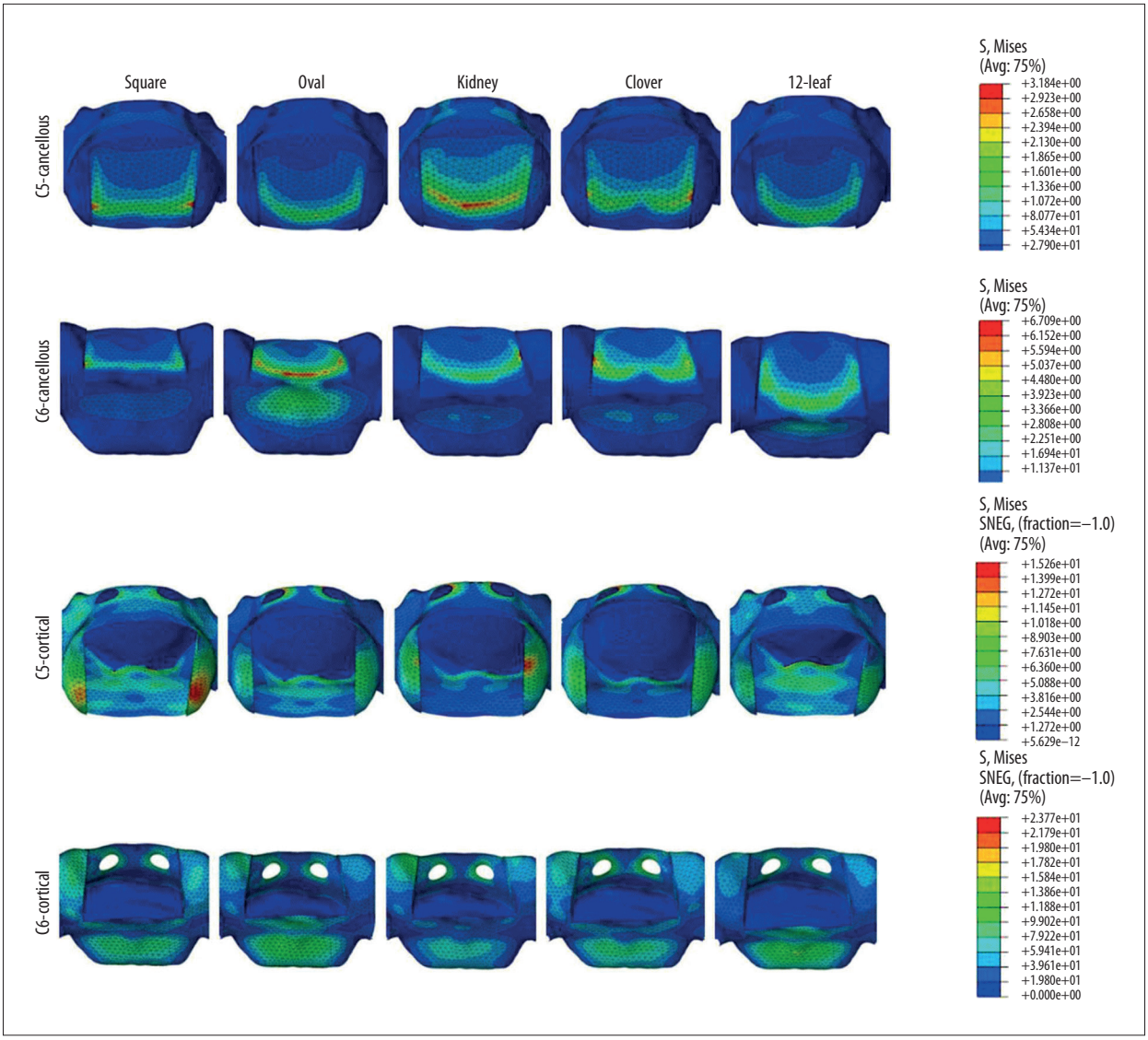


**Figure 9.** Stress distribution on cancellous bones and cortical bones of the five shapes of the cervical intervertebral cages in the extension motion condition.

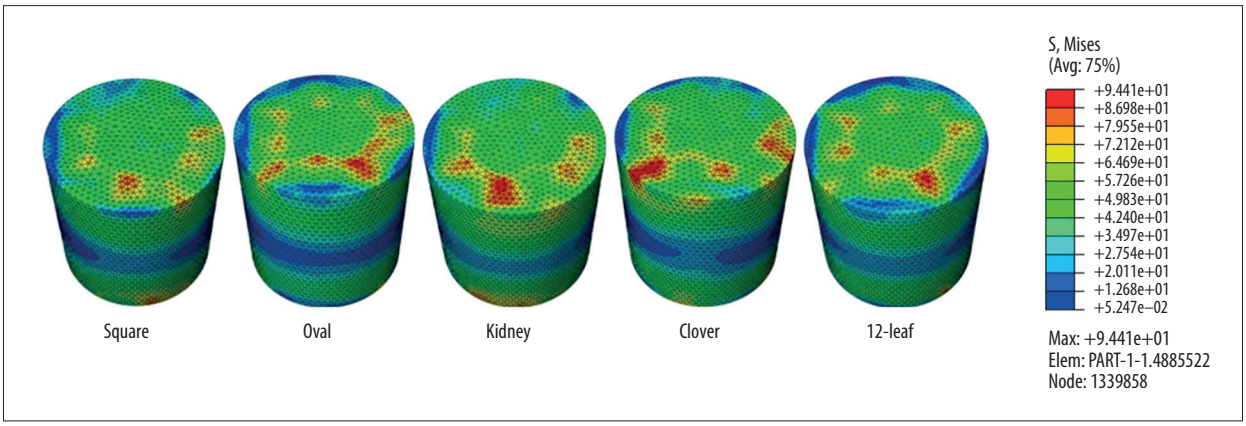


**Figure 10.** Stress distribution on bone grafts of the five shapes of the cervical intervertebral cages in the extension motion condition.





Indexed in: [Current Contents/Clinical Medicine] [SCI Expanded] [ISI Alerting System] [ISI Journals Master List] [Index Medicus/MEDLINE] [EMBASE/Excerpta Medica] [Chemical Abstracts/CAS]

The combination of the cage shape with the minimal effects on the stress distribution of cortical bone, in addition to the square-shaped and kidney-shaped fusion in C5 cortical bone stress, showed a concetration of stress, whereas the other shapes failed to produce this concentration of stress concentration. Figure 10 shows the extension movement state and the surface stress distributions of the five kinds of bone graft fusion shapes. The maximum stress was mainly distributed on the contact surface with the vertebral body. For the oval shape, kidney shape, clover shape, and 12-leaf shape of fusion cages, the stress distribution areas were large and could stimulate rapid vertebral body bone graft fusion.

## Discussion

In this study, finite element (FE) simulation was used to investigate the mechanical properties of the cervical fusion interbody device, or cervical intervertebral fusion cage, and its ability to prevent subsidence and its performance in bone graft fusion. Compared with extension, lateral bending, and rotation motion modes, the axial compression, and forward bending movement modes showed a lower risk of subsidence during fusion but a greater possibility of bone graft fusion. For patients with anterior cervical fusion surgery, postoperative stationery positioning and forward bending motion reduced the possibility of subsidence but did not have beneficial effects on fusion. Extension, lateral bending, and rotation resulted in increased graft stress to promote bone graft fusion but increased the risk of the occurrence of subsidence.

The evaluation of postoperative motion patterns and cage shape showed that in extension, lateral bending, and rotation modes, the influence of the shape of the fusion cages significantly changed its mechanical properties. In contrast, the influence of axial compression and the state of the forward bending motion was not significant. Therefore, the study demonstrated that movement patterns significantly influenced the mechanical properties of the implant, which was consistent with the findings from previous studies [30,31]. The12-leaf shape of the intervertebral fusion cage, similar to the optimum shape designed by Hsu [14], showed good resistance to subsidence.

Analysis of the stress distribution showed that in the extension movement mode, all shapes of cage showed an edge stress concentration phenomenon, according to the stress distribution analysis. The 12-leaf cage showed good mechanical properties that may have been associated with the surface of the leaf shapes, which has a large edge length that avoided the edge stress concentration effect. Analysis of the fusion effect showed that the 12-leaf cage reduced the stress on the surrounding tissues and the stress on the corresponding bone graft, which adversely affected fusion. This phenomenon may be related to the stress distribution on the edge of the fusion area.

This study had several limitations. This study used a simplified model, and the material properties of the vertebra, bone graft, and cage were modeled as isotropic linear elements. Also, the screws were modeled as solid cylinders which bound to the vertebrae and the plate, and the threads of the screws were not included in the analysis [32]. Also, due to the lack of *in vivo* or *in vitro* experimental studies, including stress responses, the ACPC models established in this study remain to be verified by experimental data. Therefore, the results obtained from the models described in this study should be interpreted with caution. It was not possible to completely duplicate the findings from *in vivo* studies using FE analysis [33]. Despite the above limitations, this study effectively demonstrated the biomechanical changes associated with the different shapes of cages in ACPC by maintaining the consistency of the experimental conditions of each ACPC model.

## Conclusions

There have been no previous studies on the postoperative effects of different shapes of the cervical intervertebral fusion cage under different physiological motion patterns. This study aimed to use finite element (FE) parametric analysis to compare biomechanical properties of changes in intervertebral cage shape for C5–C6 cervical fusion using the anterior cervical plate and cage (ACPC) fixation system. Five cage shapes were studied, including square, oval, kidney-shaped, clover-shaped, and 12-leaf-shaped. The results showed that the 12-leaf shape of the cage resulted in the optimal postoperative resistance to subsidence, and the kidney shape resulted in the optimal postoperative fusion. The FE analysis method may be useful for future developments in the design of spinal implants.

### Conflict of interest

None.





Indexed in: [Current Contents/Clinical Medicine] [SCI Expanded] [ISI Alerting System] [ISI Journals Master List] [Index Medicus/MEDLINE] [EMBASE/Excerpta Medica] [Chemical Abstracts/CAS]

## References:

1. Liu C, Liu K X, Chu L et al: Posterior percutaneous endoscopic cervical discectomy through lamina-hole approach for cervical intervertebral disc herniation. Int J Neurosci, 2019; 129(7): 627–34
2. Balasa A, Bielecki M, Prokopienko M et al: Lateral approach for recurrent unilateral cervical radiculopathy after anterior discectomy with fusion. Report of two cases. Wideochir Inne Tech Maloinwazyjne, 2019; 14(2): 348–52
3. Eco LC, Brayton A, Whitehead WE et al: Reconstruction of the anterior craniocervical junction using an expandable cage after resection of a C1 chordoma in a 5-year-old child: case report. J Neurosurg Pediatr, 2019; 24(1): 62–65
4. Alvi MA, Kurian SJ, Wahood W et al: Assessing the difference in clinical and radiologic outcomes between expandable cage and nonexpandable cage among patients undergoing minimally invasive transforaminal interbody fusion: A systematic review and meta-analysis. World Neurosurg, 2019; 127: 596–606
5. Goz V, Buser Z, D'Oro A et al: Complications and risk factors using structural allograft versus synthetic cage: Analysis 17783 anterior cervical discectomy and fusions using a national registry. Global Spine J, 2019; 9(4): 388–92
6. Oliver JD, Goncalves S, Kerezoudis P et al: Comparison of outcomes for anterior cervical discectomy and fusion with and without anterior plate fixation: A systematic review and meta-analysis. Spine, 2018; 43(7): E413–22
7. Fernandez-Fairen M, Alvarado E, Torres A: Eleven-year follow-up of two cohorts of patients comparing stand-alone porous tantalum cage versus autologous bone graft and plating in anterior cervical fusions. World Neurosurg, 2019; 122: E156–67
8. Noordhoek I, Koning MT, Vleggeert-Lankamp CLA: Evaluation of bony fusion after anterior cervical discectomy: a systematic literature review. Eur Spine J, 2019; 28(2): 386–99
9. Kettler A, Wilke H J, Claes L: Effects of neck movements on stability and subsidence in cervical interbody fusion: An *in vitro* study. J Neurosurg, 2001; 94(1 Suppl.): 97–107
10. Lu T, Liang H, Liu C et al: Effects of titanium mesh cage end structures on the compressive load at the endplate interface: A cadaveric biomechanical study. Med Sci Monit, 2017; 23: 2863–70
11. Tan JS, Bailey CS, Dvorak MF et al: Interbody device shape and size are important to strengthen the vertebra – implant interface. Spine, 2005; 30(6): 638–44
12. Yang K, Teo EC, Fuss FK: Application of Taguchi method in optimization of cervical ring cage. J Biomech, 2007; 40 (14): 3251–56
13. Kandziora F, Schollmeier G, Scholz M et al: Influence of cage design on interbody fusion in a sheep cervical spine model. J Neurosurg, 2002; 96(3 Suppl.): 321–32
14. Hsu CC: Shape optimization for the subsidence resistance of an interbody device using simulation-based genetic algorithms and experimental validation. J Orthop Res, 2013; 31(7): 1158–63
15. Wang J, Qian Z, Ren L et al: [A dynamic finite element model of human cervical spine with *in vivo* kinematic validation.] Chinese Science Bulletin 2014; 59(33): 4578–88 [in Chinese]
16. Zhang QH, Teo EC, Ng HW et al: Finite element analysis of moment-rotation relationships for human cervical spine. J Biomech, 2006; 39(1): 189–93
17. Ha SK: Finite element modeling of multi-level cervical spinal segments (C3–C6) and biomechanical analysis of an elastomer-type prosthetic disc. Med Eng Phys, 2006; 28: 534–41
18. Ng HW, Teo EC: Nonlinear finite-element analysis of the lower cervical spine (C4–C6) under axial loading. J Spinal Disord, 2001; 14: 201–10
19. Kallemeyn N, Gandhi A, Kode S et al: Validation of a C2–C7 cervical spine finite element model using specimen-specific flexibility data. Med Eng Phys, 2010; 32: 482–89
20. Panzer MB, Cronin DS: C4–C5 segment finite element model development, validation, and load-sharing investigation. J Biomech, 2009; 42: 480–90
21. Shea M, Edwards WT, White AA et al: Variations of stiffness and strength along the human cervical spine. J Biomech, 1991; 24(2): 95–107
22. Yoganandan N, Kumaresan SC, Voo L et al: Finite element modeling of the C4–C6 cervical spine unit. Med Eng Phys, 1996; 18(7): 569–74
23. Heitplatz F, Hartle SL, Gentle CR: A 3-dimensional large deformation FEA of a ligamentous C4–C7 spine unit. Comput Method Biomech, 1999; 2: 387
24. Teo EC, Ng HW: Evaluation of the role of ligaments, facets and disc nucleus in lower cervical spine under compression and sagittal moments using finite element method. Med Eng Phys, 2001; 23(3): 155–64
25. Moroney SP, Schultz AB, Miler JAA et al: Load-displacement properties of lower cervical spine motion segments. J Biomech, 1988; 21(9): 769–79
26. Teo EC, Yang K, Fuss FK et al: Effects of cervical cages on load distribution of cancellous core – a finite element analysis. J Spinal Disord Tech, 2004; 17(3): 226–31
27. Chen SH, Zhong ZC, Chen CS et al: Biomechanical comparison between lumbar disc arthroplasty and fusion. Med Eng Phys, 2009; 31(2): 244–53
28. Closkey RF, Parsons JR, Lee CK et al: Mechanics of interbody spinal fusion. Analysis of critical bone graft area. Spine, 1993; 18(8): 1011–15
29. Pearcy MJ, Evans JH, O'Brien JP: The load bearing capacity of vertebral cancellous bone in interbody fusion of the lumbar spine. Eng Med, 1983; 12(4): 183–84
30. Natarajan RN, Chen BH, An HS et al: Anterior cervical fusion: A finite element model study on motion segment stability including the effect of osteoporosis. Spine, 2000; 25(8): 955–61
31. Chiang MF, Teng JM, Huang CH et al: Finite element analysis of cage subsidence in cervical interbody fusion. J Med Biol Eng, 2004; 24(4): 201–8
32. Meng L, Zhang Y, Lu Y: Three-dimensional finite element analysis of miniexternal fixation and Kirschner wire internal fixation in Bennett fracture treatment. Orthop Traumatol Surg Res, 2013; 99(1): 21–29
33. Ouyang PR, Lu T, He XJ et al: Biomechanical comparison of integrated fixation cage versus anterior cervical plate and cage in anterior cervical corpectomy and fusion (ACCF): A finite element analysis. Med Sci Monit, 2019; 25: 1489–98





Indexed in: [Current Contents/Clinical Medicine] [SCI Expanded] [ISI Alerting System] [ISI Journals Master List] [Index Medicus/MEDLINE] [EMBASE/Excerpta Medica] [Chemical Abstracts/CAS]